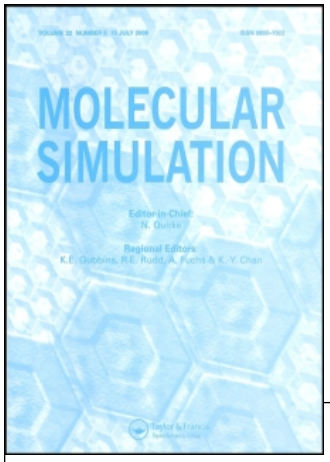

Molecular Simulation
Publication details, including instructions for authors and subscription information:
http://www.informaworld.com/smpp/title~content=t713644482

Disaccharide conformational maps: adiabaticity in analogues with variable ring shapes

Carlos A. Stortz [a]; Alfred D. French [b]

[a] Departamento de Química Orgánica-CIHIDECAR, Fac. Ciencias Exactas y Naturales, Universidad de Buenos Aires, Buenos Aires, Argentina
[b] Southern Regional Research Center, US Department of Agriculture, New Orleans, LA, USA

Online Publication Date: 01 April 2008

To cite this Article: Stortz, Carlos A. and French, Alfred D. (2008) 'Disaccharide conformational maps: adiabaticity in analogues with variable ring shapes', Molecular Simulation, 34:4, 373 — 389

To link to this article: DOI: 10.1080/08927020701663339
URL: http://dx.doi.org/10.1080/08927020701663339

Molecular Simulation
Vol. 34, No. 4, April 2008, 373–389

Disaccharide conformational maps: adiabaticity in analogues with variable ring shapes

Carlos A. Stortz[a]* and Alfred D. French[b]*

[a]*Departamento de Química Orgánica-CIHIDECAR, Fac. Ciencias Exactas y Naturales, Universidad de Buenos Aires, Buenos Aires, Argentina;* [b]*Southern Regional Research Center, US Department of Agriculture, New Orleans, LA, USA*

(*Received 28 June 2007; final version received 4 September 2007*)

Relaxed MM3 φ, ψ potential energy surfaces (conformational maps) were calculated for analogues of α,α-trehalose, β,β-trehalose, α,β-trehalose, maltose, cellobiose and galabiose based on 2-methyltetrahydropyran. Starting structures included not only $^4C_1$ (sugar nomenclature) geometries, but also combinations with $^1C_4$ conformers, and some flexible (boat or skew) forms. These forms were included as part of continuing efforts to eliminate unwarranted assumptions in modelling studies, as well as to account for new experimental findings. Four to nine maps were obtained for each analogue, and from them adiabatic maps were produced. Although the minimum energy regions always resulted from $^4C_1$—$^4C_1$ geometries, moderate to large parts of most maps had lower energies when one or both rings were in the $^1C_4$ conformation. Only the adiabatic surface for the (diequatorial) analogue of β,β-trehalose was covered entirely by $^4C_1$—$^4C_1$ conformers. For the cellobiose and α,β-trehalose analogues, these conformers covered 74 and 67% of the surfaces, respectively. The remainder of the cellobiose analogue surface was covered by conformers having a $^1C_4$ conformation at the "reducing" end, and for the α,β-trehalose analogue, by conformers having $^1C_4$ shapes for the α-linked unit. Adiabatic surfaces of the other three analogues were based on all combinations of $^4C_1$ and $^1C_4$ conformers. The "normal" $^4C_1$—$^4C_1$ combination only covered 37–41% of those surfaces, whereas each of the other three conformations accounted for 10–31%. Although the "normal" conformation accounted for 97.0–99.8% of the total population, adiabaticity in disaccharide maps is not guaranteed unless variable ring shapes (another manifestation of the "multiple minima problem") are considered.

Keywords: carbohydrate; cellobiose; galabiose; maltose; tetrahydropyran; trehalose

1. Introduction

Knowledge of the conformations of disaccharides is important because their shapes are key to understanding their properties. Also, that information can be extrapolated to oligo- and poly-saccharides having the same primary structure [1]. One way to study conformational probability is to generate a Ramachandran-like conformational map, where the energy is determined for all mutual orientations of the two monosaccharide residues, as expressed by their glycosidic torsion angles φ and ψ [2–5]. If the maps are of sufficient quality, real structures should occur in regions of low energy. Besides the energies of minima, these maps also allow assessment of the distortion energies of experimental structures (in complexes with enzymes and other proteins, for example [6]) as well as the barriers between different minima.

Originally, maps were made using rigid monosaccharide residues, but in 1979 Melberg and Rasmussen [7–9] initiated a limited type of flexible residue analysis. By the late 1980s, numerous maps based on the energies for relaxed[1] disaccharides had been constructed [3,10–14].

Adiabatic maps incorporate the lowest-energy value found at each increment of φ and ψ. As realised early on [2], the orientations of primary and secondary hydroxyl groups affect the energy. To assure that the lowest energy has been found at each point on the map, it is necessary to consider the various possible arrangements of the exocyclic groups. This "multiple minimum" problem should be addressed in all attempts to model any molecule with rotatable exocyclic groups [5]. Although not every combination of exocyclic group orientations ("starting geometry") will give rise to any low energy points, it is likely that tens or hundreds will contribute to the adiabatic map. An accompanying paper in this issue illustrates the importance of using many different combinations of exocyclic group orientations in adiabatic mapping [15]. Early studies selected one or just a few attractive starting geometries, hoping that this simplification would not impact the results more adversely than other approximations made in the study. Some current studies include a substantial number of these starting geometries, but it is still not clear if a sufficient number of exocyclic group orientations are being included.

In our relaxed φ, ψ mapping studies, we have found that sometimes the normal chair forms of the rings become deformed [15]. Such deformations are often elastic but in some instances, energy barriers are crossed, resulting in plastic transitions to flexible skew forms [6]. When those non-chair rings are used as the starting geometry for minimisation at subsequent points in a scan of φ, ψ space,

*Corresponding authors. Emails: stortz@qo.fcen.uba.ar; afrench@srrc.ars.usda.gov

ISSN 0892-7022 print/ISSN 1029-0435 online

DOI: 10.1080/08927020701663339
http://www.informaworld.com

they will usually not return to the original chair shape. For example, a chair-form ring is used as the starting structure for minimisation at $\varphi = 0°$. Suppose that at $\varphi = 120°$, the ring changed during minimisation to a skew form. If that skew-form ring were used as the starting geometry for the next optimisation at $\varphi = 130°$, that optimisation would probably not return the ring to the chair shape, nor would the optimisations at succeeding points, including that at $\varphi = 360°$. Therefore, the calculated energy value at $\varphi = 360°$ will differ from what it was at 0°, an undesirable, seemingly illogical result. This behaviour leads to similar consequences as those from spontaneous rotation of exocyclic groups during minimisation of actual disaccharides.

While these plastic deformations are useful for finding new geometries with lower energy for some parts of the energy maps, many will lead to subsequent points on the surface with energies higher than those that would have been generated if the original, well-chosen starting structure had been used at each φ, ψ grid point. However, if minimisations at all φ, ψ grid points start with only the lowest-energy initial ring shape, the lower energy that could be provided at some φ, ψ points by the deformed alternative ring shape will not be found unless deformation occurs spontaneously during minimisation. Thus, when searching for the lowest energy at each φ, ψ point, it is necessary, in general, to start not only with the overall lowest-energy ring form but also with other conformations. Otherwise, the adiabaticity of the energy surface is not guaranteed. The purpose of this work is to clarify the role of ring shape when making adiabatic maps.

In previous studies [16–18] analogues of disaccharides (i.e. those with the hydroxyl groups replaced by hydrogen atoms) were used as a way of reducing the lengthy QM calculation times and avoiding the need to consider alternative rotatable exocyclic conformations. It has been shown that even without the hydroxyl groups, overall features of those maps were fairly predictive for experimentally determined shapes of the actual disaccharides, indicating that torsional energies and the bulk of the ring structures are the major factors in determining disaccharide conformations.

Herein we present 360 × 360° relaxed maps of six analogues, namely those of α,α-trehalose (**1**), β,β-trehalose (**2**), α,β-trehalose (**3**), maltose (**4**), cellobiose (**5**) and galabiose (**6**) where the hexose residues were replaced by 2-methyltetrahydropyran units. These six analogues were chosen as models of non-reducing and reducing disaccharides that normally have glycosidic linkage bonds that are both equatorial, both axial, or a combination of one axial and one equatorial. Besides reducing the scope and the time required for the project, using the analogues allowed us to focus on the role of ring shape in adiabatic mapping as well as to demonstrate an approach to learning about that role.

Energies were calculated using four different conformers as starting geometries: one consisting of both normal chairs, another with both alternate chairs ($^1C_4$, using carbohydrate nomenclature), and the other two having one normal and one alternate chair. For **1** and **2**, five additional maps were made with structures having boat/skew starting conformations. From all of these data, the adiabatic maps were generated, and the necessity of using alternative ring shapes in further calculations is discussed. Also, the differences in the maps for the different combinations of ring shapes are noted. This is helpful for understanding experimental results for molecules such as permethylated cyclomaltoheptaose, which in one crystal structure incorporates one glucose ring with a $^1C_4$ shape as well as six $^4C_1$ rings [19].

Although QM mapping studies of some hydroxyl-bearing disaccharides have been carried out [15,20–22], the energies herein were calculated with the MM3 empirical force field software [23] (details are in the Methods section, at the end of the paper). This is a general, all-atom force-field with parameterisation of anomeric effects and hydrogen bonding as required for carbohydrates. Previous work showed a reasonable correspondence between MM3 and quantum mechanics results for variations in ring shape, especially for analogues [24]. The present approach could also be used with other methods of energy calculation, including quantum mechanics, with or without continuum solvation. Exploration of alternative ring shapes with molecular dynamics may require the application of metadynamics or a similar methodology [25].

2. Nomenclature

The non-hydroxylated analogues of α,α-trehalose (**1**), β,β-trehalose (**2**), α,β-trehalose (**3**), maltose (**4**), cellobiose (**5**) and galabiose (i.e. α-Gal(1,4)Gal) (**6**), are shown in Figure 1. Their systematic names are 6-methyl-2-(6′-methyltetrahydropyran-2′-yloxy) tetrahydropyran as the (2*R*,2′*R*, 6*R*,6′*R*) (**1**), (2*S*,2′*S*,6*R*,6′*R*) (**2**), and (2*R*,2′*S*,6*R*,6′*R*) (**3**) diastereomers, and 2-methyl-3-(6′-methyltetrahydropyran-2′-yloxy)tetrahydropyran as the (2*R*,2′*R*,3*S*,6′*R*) (**4**), (2*R*,2′*S*,3*S*,6′*R*) (**5**), and (2*R*,2′*R*,3*R*,6′*R*) (**6**) diastereomers. The numbering is based on carbohydrate nomenclature, with the anomeric carbon as C1 and C5 carrying the methyl group.

For **1**, **2**, and **3**, φ and ψ are defined by atoms O5′–C1′–O1′–C1 and C1′–O1′–C1–O5, respectively. For **1** and **2**, maps should be symmetrical about a line where $\varphi = \psi$. For **3**, the α-unit was arbitrarily chosen to define the φ angle. For **4**, **5** and **6**, φ and ψ are defined by O5′–C1′–O1′–C4 and C1′–O1′–C4–C5, respectively.

The conformations of the methyltetrahydropyranyl ring were indicated by a single letter: **N** for the normal chair (equivalent to the $^4C_1$ conformation of

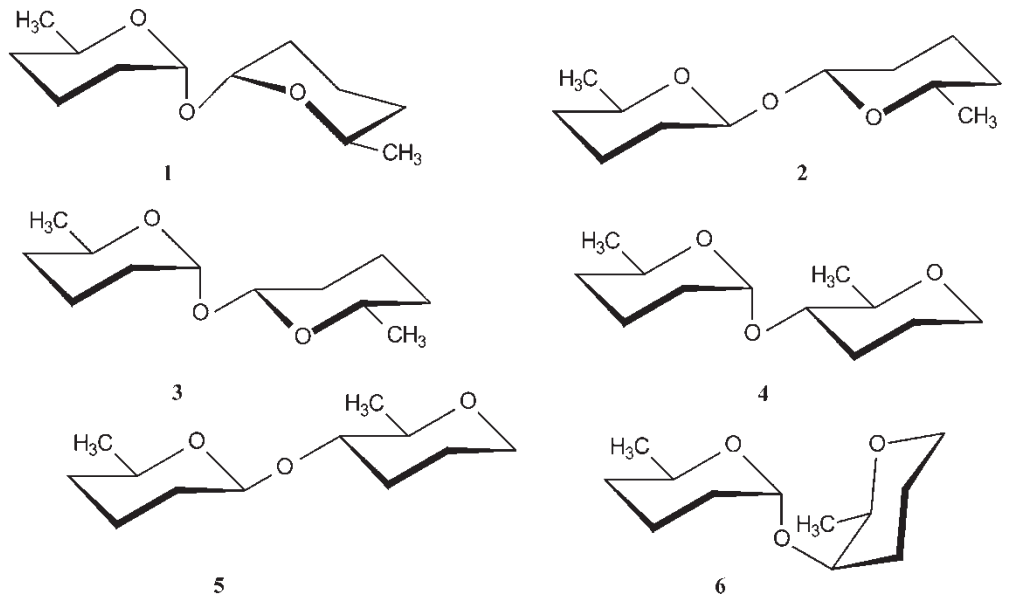

Figure 1. The compounds studied in this work.

D-glucopyranose); **A**, for the alternative chair ($^1C_4$); and **B** for a flexible skew or boat form. The selected **B** structure is near the $B_{2,5}$ conformation, which in preliminary studies proved to have the lowest energy among the flexible forms. We included only one **B** conformation because pseudorotation along the skew-boat itinerary was expected to be relatively facile for these analogues, as indicated for 2-methoxytetrahydropyran [24]. (Later, we found that facile pseudorotation was not always a particularly useful assumption.) The Cremer-Pople [26] θ values for "perfect" **N**, **B** and **A** conformers are 0, 90 and 180°, respectively. We ignored the **E** and **H** conformations because they are unstable for these compounds. Therefore, all structures with θ between 40 and 125° were classified as **B** conformers. Our range was asymmetric because calculated θ values were fairly continuous between 90 and 180°, whereas in the Southern hemisphere, there were only a few values near 40°, making it a good cut-off value. The $\theta = 125°$ value corresponds to the Northern **E** form which should ordinarily correspond to a transition state (e.g. a carbenium ion).

For the present analogues, the acronym for the conformation contains the letter for the "non-reducing" residue followed by that of the "reducing" one, e.g. the **AN** conformer of **5** is the cellobiose analogue with the glycosidically linked unit in the alternate chair conformation and the aglycon in the normal chair conformation. As changing from the **A** to the **N** form redefines the axial or equatorial orientation of the glycosidic linkage bonds (or equivalent in the flexible forms), it was sometimes convenient to use lowercase letters in italics following the **A/N** designations to indicate axial (*a*) and equatorial (*e*) linkage geometries.

3. Results

The nine conformers of compound **1** (octadeoxy α,α-trehalose) were combinations of the normal (equivalent to $^4C_1$) and alternate chairs, and a boat-like structure (see Nomenclature). Each made its own map, designated **AA** (*e,e*), **AB**, **AN** (*e,a*), **BA**, **BB**, **BN**, **NA** (*a,e*), **NB** and **NN** (*a,a*). At some grid points, **NN** starting geometries were plastically deformed. Also, because the MM3 dihedral driver 4 does not carry deformed rings forward to the next grid points, some very high relative energies occurred (i.e. more than 100 kcal above the global minimum, sometimes 1000 kcal above). In those conformations, the monosaccharide units practically interpenetrate each other, making meaningful minimisation impossible [6]. Because we had increased the glycosidic valence bond angle for the starting structures to 150° (instead of that expected for a glycosidic angle, around 115°) this problem of unreasonable structures and energies was greatly diminished [6]. The high symmetry of the **AA**, **BB** and **NN** maps as well as the similarity of the equivalent maps (e.g. **AB** and **BA** after turning 90°) indicated that the calculations proceeded correctly. Furthermore, no very high energy points were encountered for eight of the nine maps: the **NN** map had 21 (out of 1296) grid points with very high energy (Table 1). Maps for the individual starting structures were contoured without including values for those high-energy φ, ψ points, but their locations have been indicated.

All of the rings with alternate chair conformations retained their shape during the grid search (Table 1). Even with the **NN** starting geometries, 1236 out of the 1296 calculations led to **NN** conformers with reasonable energies, and fewer than 40 of the normal chairs switched to boats. However, the **A** chairs, with equatorial C1—O1 bonds, remained almost unaltered by minimisation: their average θ puckering value was 176°, with extreme values of 171 and 180°. On the other hand, at some points **N** chairs showed marked distortions towards envelopes or half chairs (around $\mathbf{E}_5$, i.e. C2 was brought into the plane of the O5, C1, C3 and C4 atoms), or even to boats, as described above. The average θ value was 10°, but a large range of values was observed. Our "boats" had average θ values of 89°, ranging from 87 to 90°. They stayed near the $B_{2,5}$ conformation, with an average $\Phi = 310°$, but the distribution was bimodal, with Φ values mostly for skews on either side ($^1S_5$ or $^oS_2$). Figure 2 shows the relaxed maps for the four combinations of chairs (**AA**, **AN**, **NA** and **NN**). The areas of the maps marked in red indicate where high-energy points or final conformations different from the starting form were achieved.

A similar calculation was carried out with the nine starting structures for the analogue of β,β-trehalose (**2**, Figure 1), leading to the four relaxed maps shown in Figure 3. The distribution of final conformers is shown in Table 1. For this compound, the **NN** starting conformation led to all 1296 final molecules having the same ring

Table 1. Number and type of conformations reached for the 1296 grid points of the maps of **1**–**6** starting from each different conformer.

Starting from	High-energy	**AA**	**AB**	**AN**	**BA**	**BB**	**BN**	**NA**	**NB**	**NN**
1										
AA	–	1296								
AB	–		1296							
AN	–		6	1290						
BA	–				1296					
BB	–					1296				
BN	–						1296			
NA	–				6			1290		
NB	–					1			1295	
NN	21						20		19	1236
2										
AA	71	801	140	4	146	110	9	8	7	–
AB	59		969	28		191	32		11	6
AN	22			1050			221			3
BA	39				1020	218	1	6	12	
BB	19					1232	12		31	2
BN	–						1258			38
NA	15							1049	229	3
NB	–					1			1257	39
NN	–									1296
3										
AA	17	1036	243							
AN	–			1296						
NA	61		1		11	13		975	226	9
NN	–						3			1293
4										
AA	–	1296								
AN	–			1296						
NA	14				23			1254	5	
NN	14						42			1240
5										
AA	63	961	2		249	6		15		
AN	69			950			263			14
NA	–							1296		
NN	–									1296
6										
AA	–	1296								
AN	–			1296						
NA	19				27			1250		
NN	42						41			1223

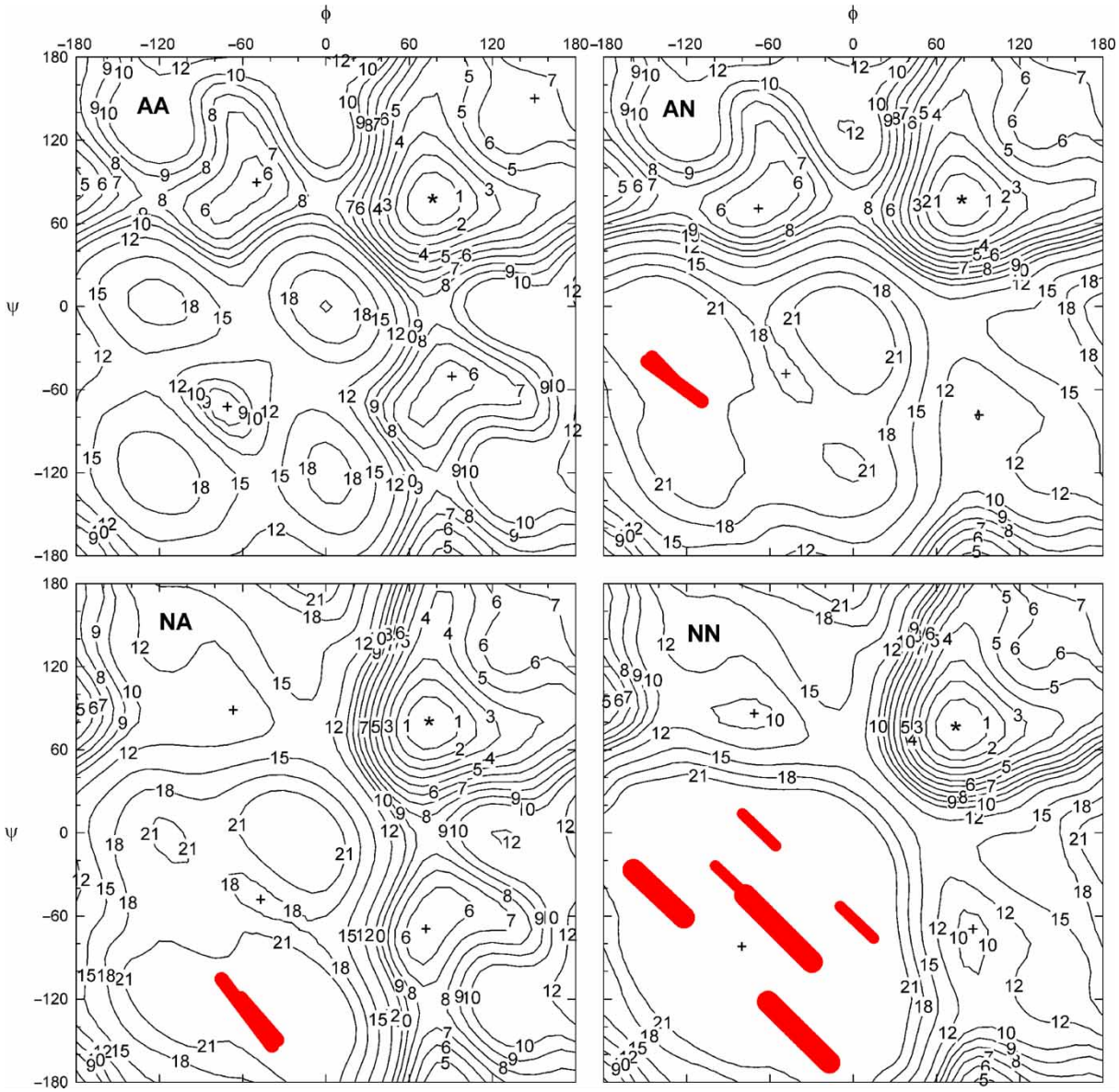

Figure 2. Contour relaxed maps for the **AA**, **AN**, **NA** and **NN** conformers of compound **1**. Iso-energy contour lines have the indicated energies, in kcal/mol. (∗) indicates the main minimum of each map, (+) other local minima. Red areas indicate regions of the map where that conformation could not be achieved at a "normal" energy.

shape. Furthermore, the rings showed very little deviation from the ideal chair, with an average θ of 5° and variations between 2 and 8°. All of the other starting geometries led to different final ring shapes at some map locations. For example, some of the starting **A** conformers led to **B** and even to **N**, and some of the starting **B** conformers ended up as **N** conformers. **A** and **B** rings also led to some high energy points (Table 1). Some of the points labelled as **A** conformers are actually severely deformed, close to ^{3}**E** conformations. The deviations from the ideal shape of the **A** conformers were pronounced, with an average θ of 167° (± 10°), with quite variable individual values. The **B** conformers also show large variations in shape: although they averaged to $\Phi = 300°$ ($B_{2,5}$), their shapes were mostly $^{1}S_5$ and $^{O}S_2$, but some were near $^{3}S_1$. The original **BB** calculations led to an unsymmetrical map. The starting structure had one skew with $^{1}S_5$ conformation and the other with $^{O}S_2$ conformation, but in many instances the barriers between them were not surmounted. Thus, a new calculation with a different starting point (with both skews in $^{1}S_5$ conformation) was made, and "mixed" with the previous one in order to obtain the relaxed map. The relaxed maps of the **AA**, **AN** and **NA** forms of **2** (Figure 3) show that large φ,ψ areas (marked in red) are not available to these conformers.

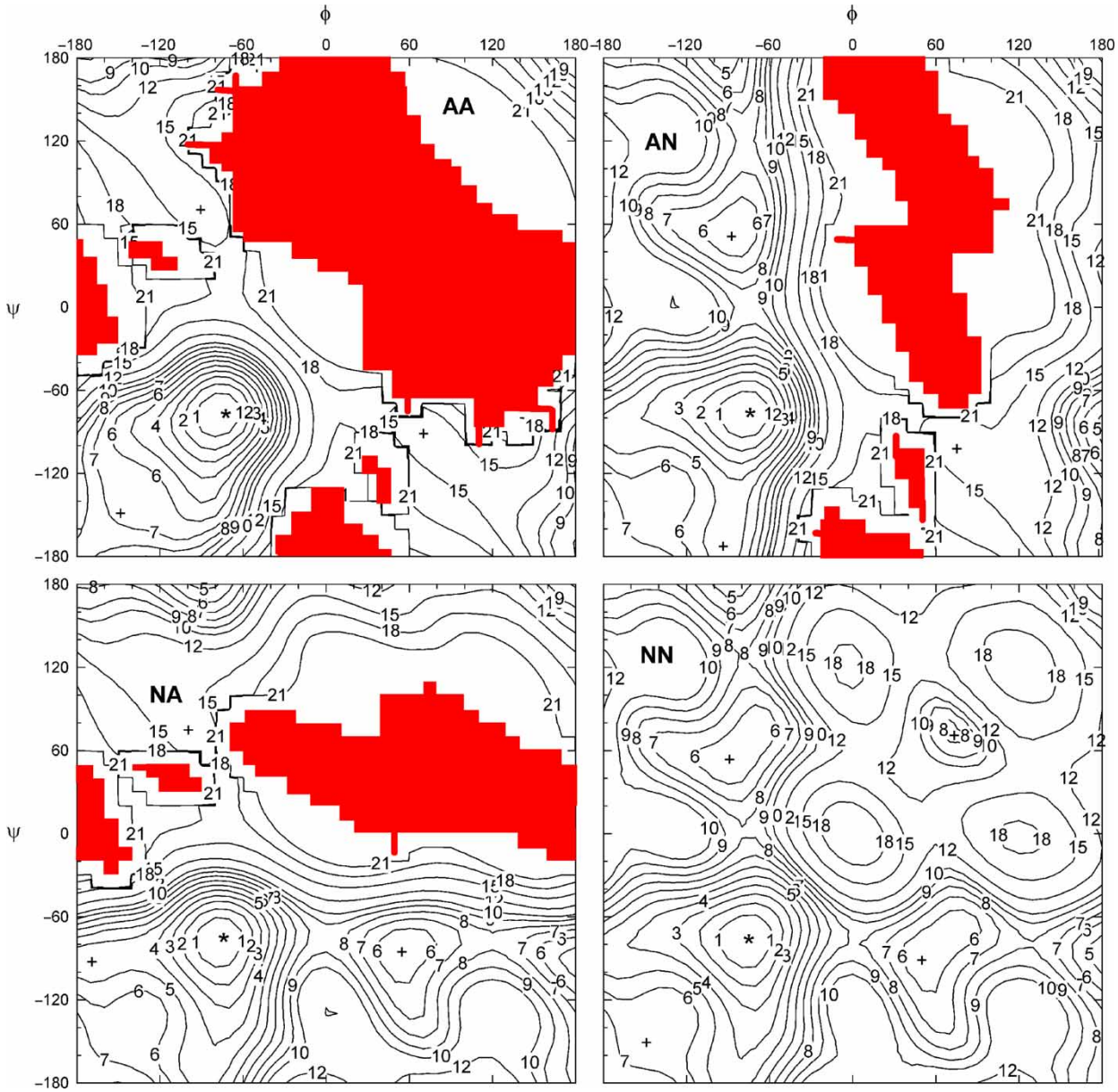

Figure 3. Contour relaxed maps for the **AA**, **AN**, **NA** and **NN** conformers of compound **2**. Iso-energy contour lines have the indicated energies, in kcal/mol. (*) indicates the main minimum of each map, (+) other local minima. Red areas indicate regions of the map where that conformation could not be achieved at a "normal" energy.

Because the flexible **B** forms for compounds **1** and **2** did not produce any points in the adiabatic maps (see below), and because these forms seemed not to be easily crossing the barriers between boats and skews, only the four combined-chair conformers were studied for the remaining compounds. The four relaxed maps for compounds **3**, **4**, **5** and **6** are shown in Figures 4–7, respectively. The number of structures of each kind resulting from the 1296 calculations for each map are shown in Table 1. As a general rule, α-linked "non-reducing" **A** rings (equatorial conformation) retained their conformations throughout the whole maps (Table 1). The same happened with the **N** conformations of β-linked units, indicating that equatorially linked glycosides experience less steric conflict and can otherwise better adapt at every point of φ, ψ space. The axial C1—O1 bonds, on the other hand, either from **N** conformations of α-linked rings or **A** forms of β-linked rings, were relatively more prone to being altered or producing very high energy structures for some φ, ψ combinations.

The "aglycon" (reducing end) is less prone to changing its shape, regardless of whether its linkage bond is equatorial or axial (Table 1). Most of these "reducing end rings" kept their starting conformations. The change of

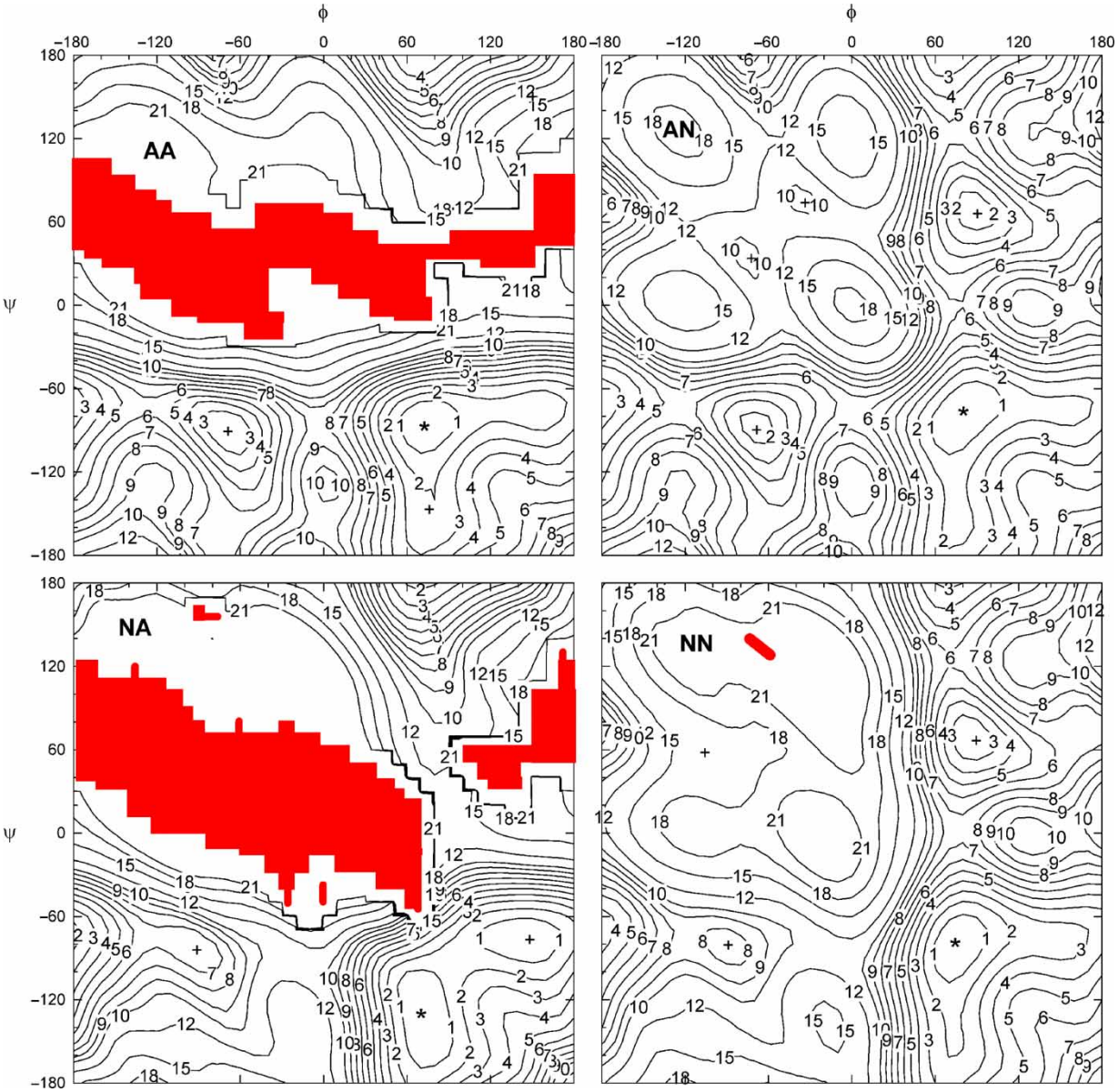

Figure 4. Contour relaxed maps for the **AA**, **AN**, **NA** and **NN** conformers of compound **3**. Iso-energy contour lines have the indicated energies, in kcal/mol. (*) indicates the main minimum of each map, (+) other local minima. Red areas indicate regions of the map where that conformation could not be achieved at a "normal" energy.

shape of the β-linked, "non-reducing" units from **N** to **A** has the largest effects on the energy surfaces. With this change, the orientations of both equatorial groups (C5 methyl and C1 oxygen) become axial. An area of φ, ψ space with the shape of a strip of constant φ (between *ca.* 0 and 60°) is prohibited for these conformers, as observed for compounds **2**, **3** and **5** (Figures 3, 4 and 6). The forbidden areas for the **N** conformers of α-linked moieties are much smaller and more scattered (Figures 2, 4, 5 and 7).

Starting from the maps in Figures 2–7, the adiabatic maps for the six compounds were generated. They are shown in Figure 8; Table 2 shows the number of contributions by each conformer to the adiabatic map. Only the adiabatic map for **2** was constructed entirely from just one conformer (**NN**, Table 2). This conformer was always the one contributing the most points to the adiabatic map, but for all other compounds large contributions of the other three conformers were also encountered. Figure 9 color-codes the adiabatic maps to indicate the regions where each conformer contributed.

Both the individual and the adiabatic maps for each compound indicate that roughly speaking, the map is divided into four parts (quadrants), each holding one or two minima. Although a three-fold "symmetry" for each

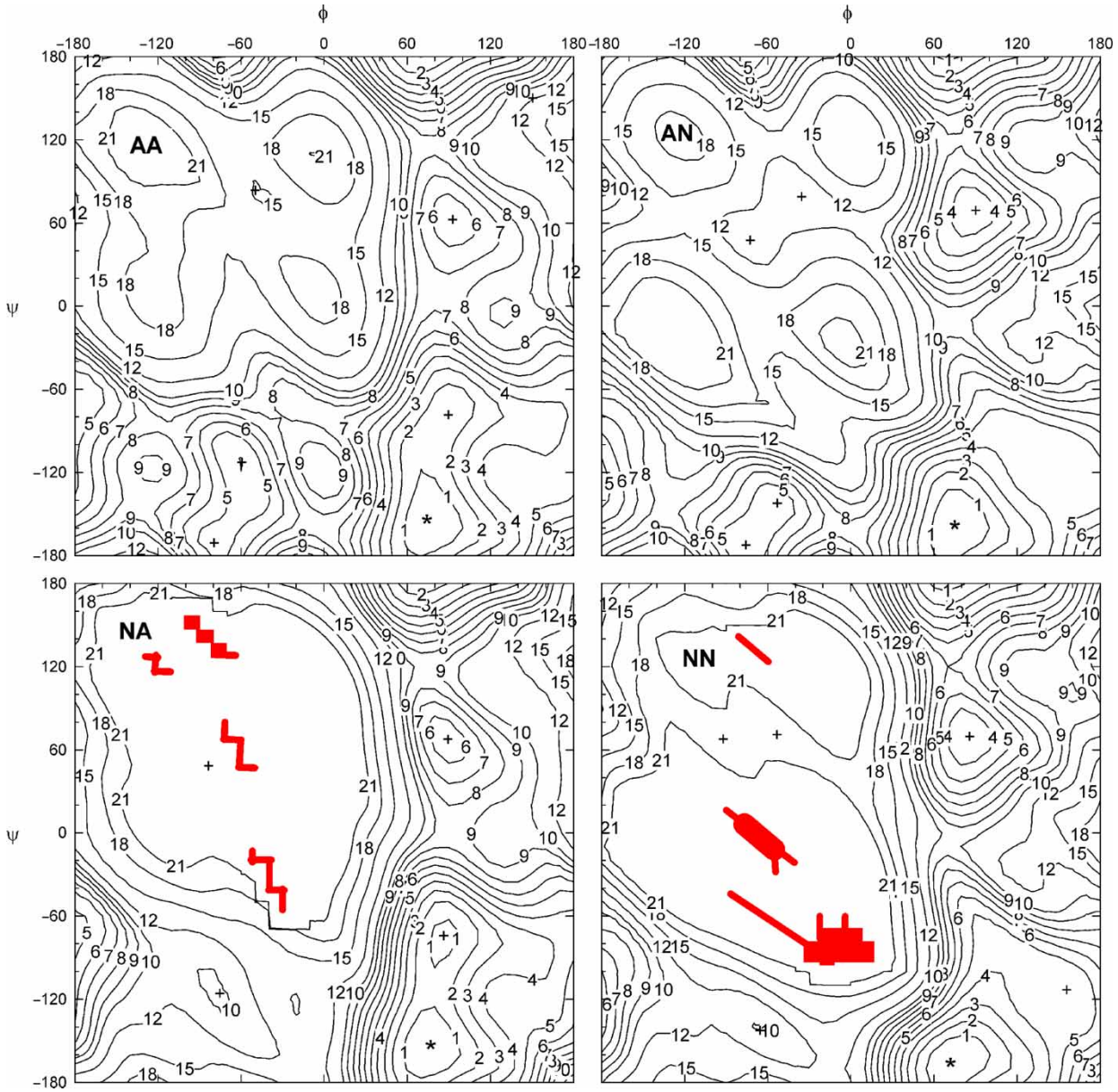

Figure 5. Contour relaxed maps for the **AA**, **AN**, **NA** and **NN** conformers of compound **4**. Iso-energy contour lines have the indicated energies, in kcal/mol. (*) indicates the main minimum of each map, (+) other local minima. Red areas indicate regions of the map where that conformation could not be achieved at a "normal" energy.

axis is expected to occur, in practice the division can be set just at φ and $\psi = 0°$, giving rise to the above mentioned four quadrants. It is implicit that a second division for each axis occurs at φ and $\psi = 180°$, in the present drawing at the edges of the maps. However, this division is less marked, and some low energy regions cross this edge. The minima found in the four quadrants for each map are listed in Tables 3 and 4 for compounds **1**–**6**. Quadrant 1 always contains the global minimum for that particular compound; Quadrant 2 was the one above or below (i.e. the same φ, different ψ); Quadrant 3 had the same ψ range as Quadrant 1 but a different φ, and Quadrant 4 was diagonally opposite to Quadrant 1. Quadrant 4 usually had the highest energies. For the symmetrical compounds (**1** and **2**) Quadrants 2 and 3 are equivalent. The four relaxed maps (for **AA**, **AN**, **NA** and **NN**) all had their global minima in the same quadrant, which was specific for each compound studied. The position of the main quadrant can be predicted just in terms of primary structure.

Table 5 shows the probability of occurrence for the four main chair variants of each compound, taking into account the full map. This indicates that many points are covered by with alternate chairs. However, the normal chairs are by far the most important when the maps are

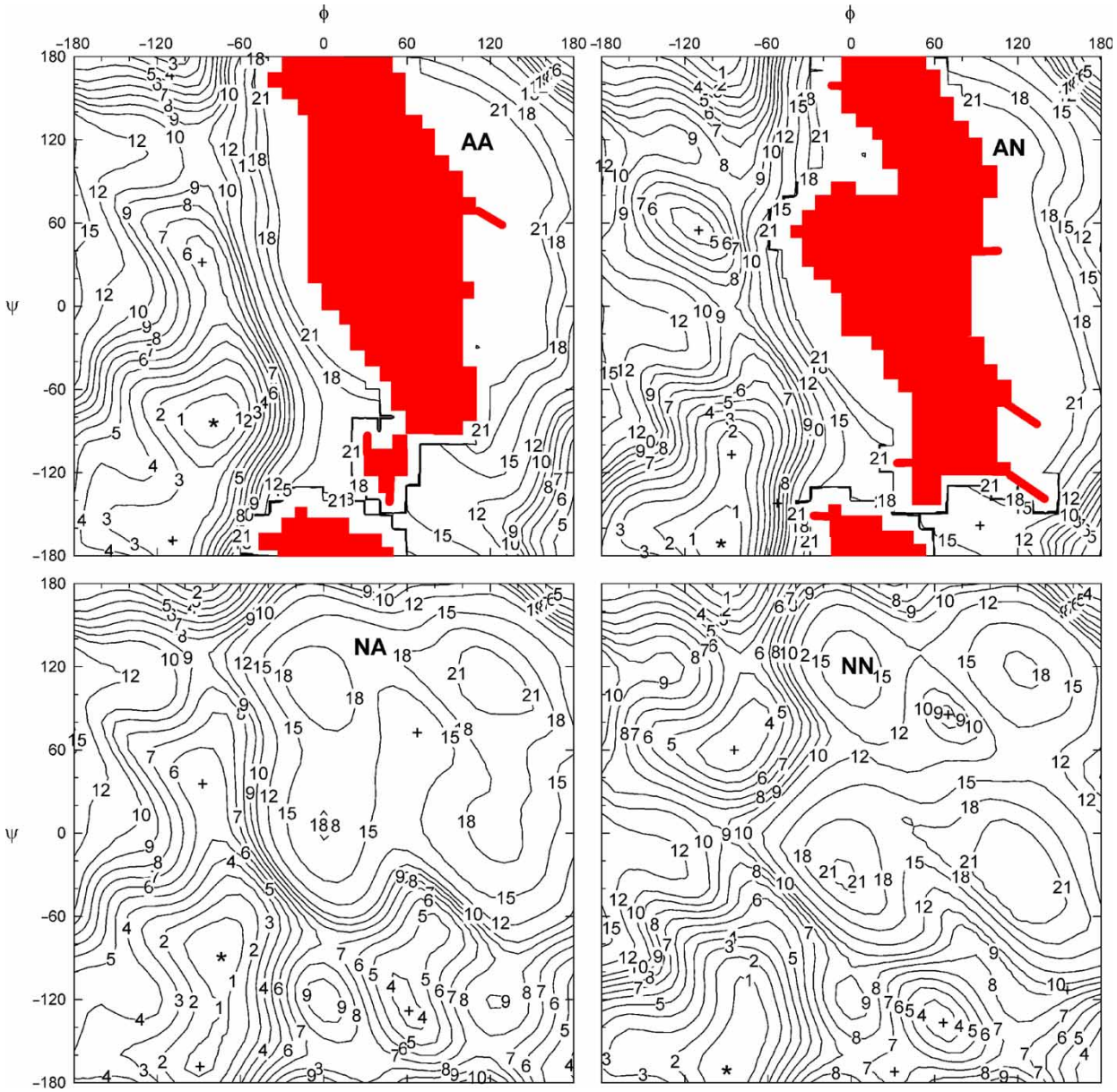

Figure 6. Contour relaxed maps for the **AA**, **AN**, **NA** and **NN** conformers of compound **5**. Iso-energy contour lines have the indicated energies, in kcal/mol. (∗) indicates the main minimum of each map, (+) other local minima. Red areas indicate regions of the map where that conformation could not be achieved at a "normal" energy.

analyzed based on Boltzmann weights. Table 6 shows the flexibilities expressed by their corrected partition functions [27] ("probability volume" [18]), with comparison to literature-reported values.

4. Discussion

As detailed in the introduction, one of the well-known problems of disaccharide mapping is the "multiple-minimum problem" that arises from the many different stable combinations of exocyclic group orientations [2,5]. However, the common assumption that the normal ($^4C_{1-D}$) chair holds for every point in the map is not always, or even usually, valid, as shown by the present work. Thus, adiabaticity is not guaranteed even when using tetrahydropyran models that lack rotatable exocyclic groups. The present work uses methyltetrahydropyran units. They should be better models of hexopyranoses than the non-methylated tetrahydropyran units, and they also should *a priori* be better stabilised in the $^4C_1$ chair than in the alternative $^1C_4$ shape because of the $^4C_1$ ring's equatorial C6 group. Without this methyl group, the proportion of alternate chairs in the maps would have undoubtedly been much higher.

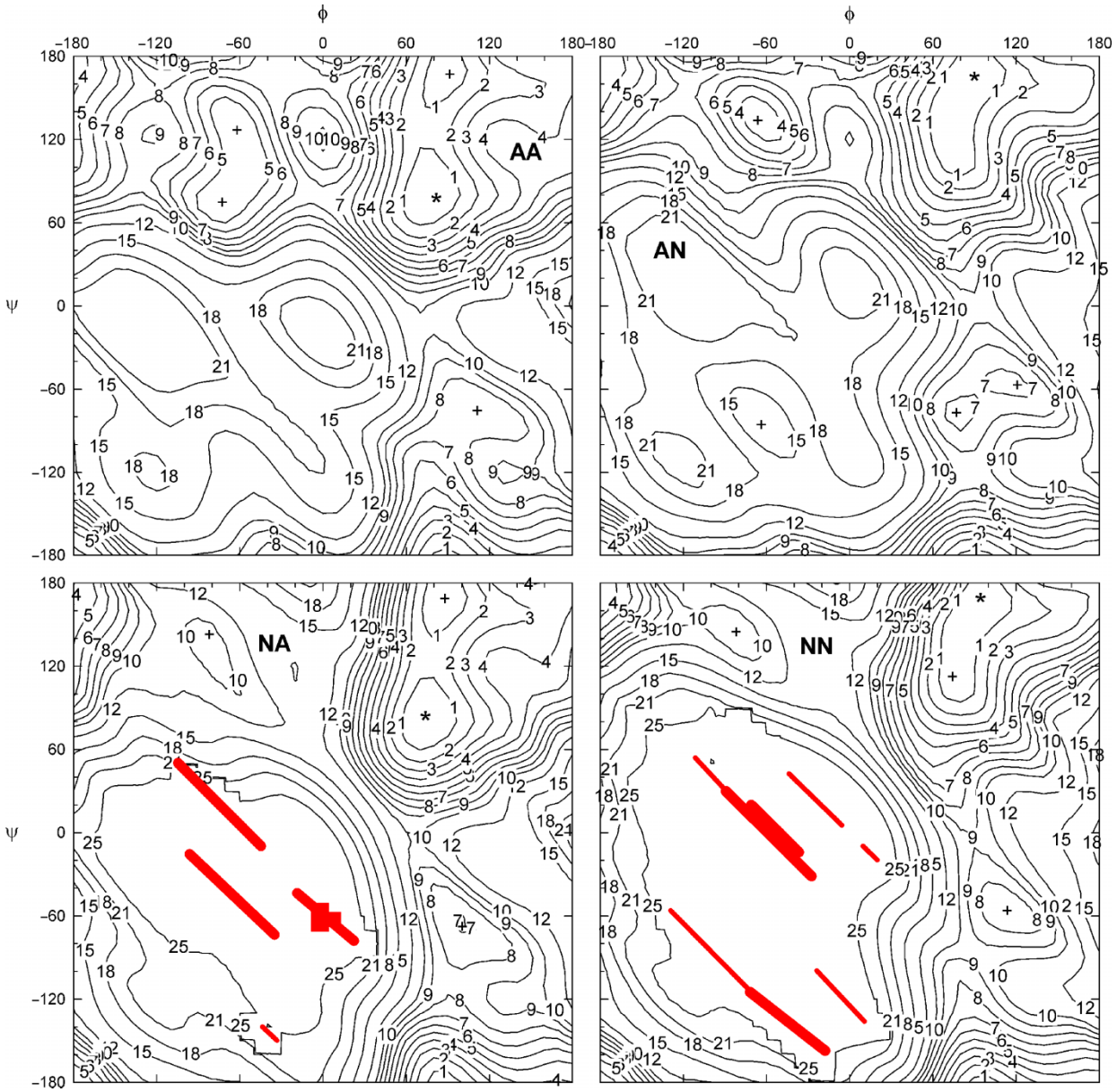

Figure 7. Contour relaxed maps for the **AA**, **AN**, **NA** and **NN** conformers of compound **6**. Iso-energy contour lines have the indicated energies, in kcal/mol. (∗) indicates the main minimum of each map, (+) other local minima. Red areas indicate regions of the map where that conformation could not be achieved at a "normal" energy.

The adiabatic maps in Figure 8 have shapes that are generally similar to those previously reported for similar compounds, with other variants of the same force-field, or using QM methods [18,28–32]. Maps for **3**–**6** have an expanded low-energy region that spans different values of ψ while keeping approximately the same φ value. The ψ span for the 2 kcal-energy region can be between 60° for **4** up to 120° for **5** or **6** (Figure 8), and sometimes also encompass a second minimum (as occurs for **6**, Table 4). The second quadrant (same φ, different ψ) contains a minimum with low energy (2–3 kcal) for compounds **3**–**5** (analogues of α,β-trehalose, maltose, and cellobiose, respectively), in which the aglycon has an equatorial linkage in its normal chair form. The secondary minimum has an intermediate energy (5 kcal) for **2**, a molecule with a diequatorial and dianomeric linkage. The Quadrant 2 minima for **1** and **6** have even higher energies (7–9 kcal), because of diaxial linkages. It has already been shown that the presence of such minima with low energy depends on having an equatorial linkage [18,33]. In the third quadrant, the cellobiose analogue gives the lowest energy minimum (**5**, Table 4, Figure 8, 3 kcal), whereas the higher energies are those for **1**, **4** and **6** (7 kcal or more) with axial anomeric bonds.

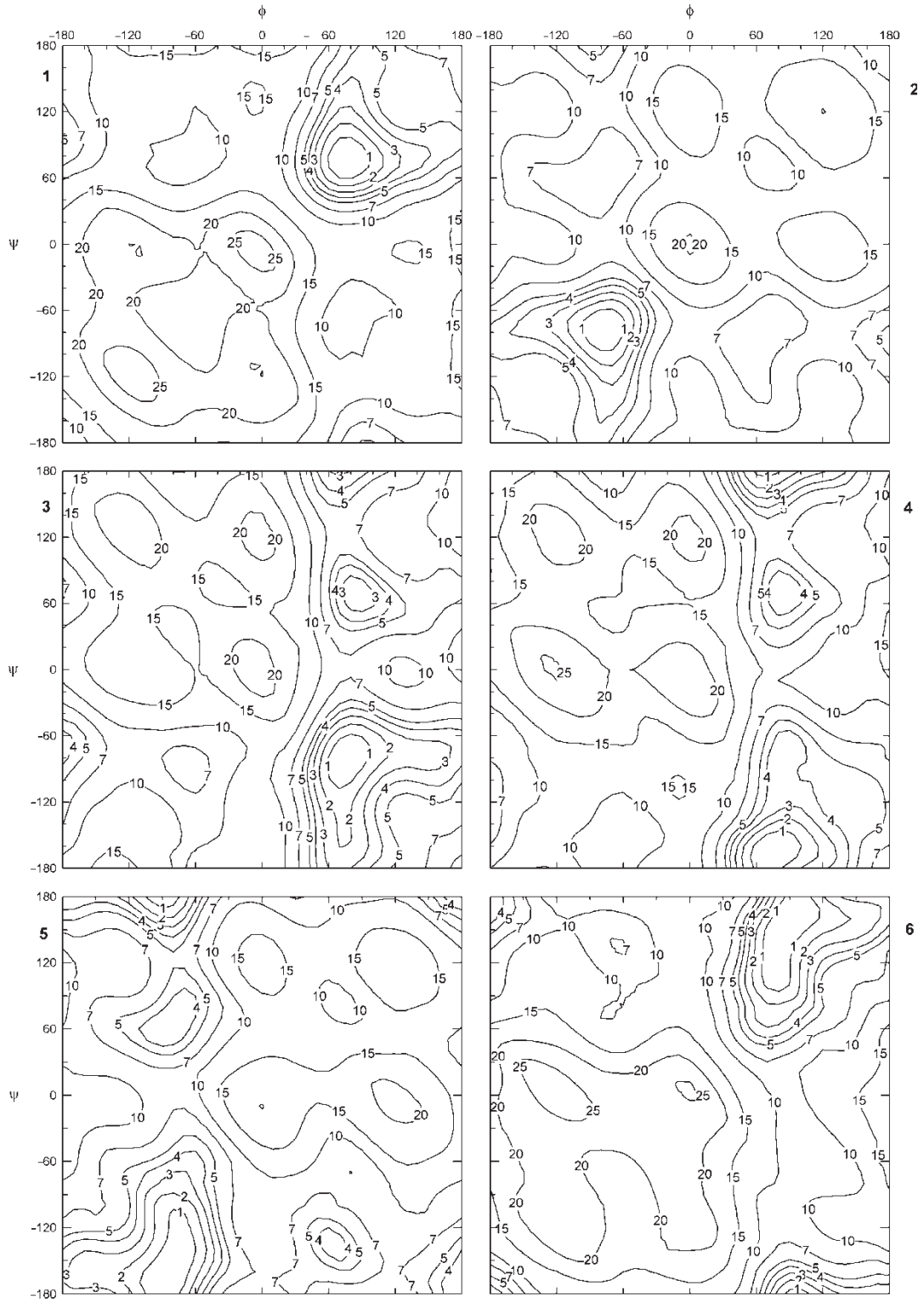

Figure 8. Adiabatic contour maps for **1**–**6**. Iso-energy contour lines have the indicated energies, in kcal/mol.

Certainly, each compound had a different quadrant 1: α-linked compounds always had it on positive φ values (towards the right), whereas β-linked compounds had it on negative φ values (to the left). However, the same occurs with the ψ angle, indicating that the reason is steric more than stereoelectronic: for compounds with an axial glycosidic linkage bond, ψ is positive; for those with equatorial bonds, ψ is negative. Actually, the axial–

Table 2. Number of grid points (total 1296) of each conformation occurring in the adiabatic map.

Compound	Conf.	**AA**	**AN**	**NA**	**NN**
1	(***a,a***)	184	290	290	532
2	(***e,e***)				1296
3	(***a,e***)		425		871
4	(***a,e***)	133	404	222	537
5	(***e,e***)			337	959
6	(***a,a***)	247	358	209	482

equatorial position has to be evaluated in the normal $^4C_1$ conformation, as the alternate ones, with a reverse axial–equatorial arrangement, also show the same behaviour. Thus, for compounds **1** and **6**, with diaxial glycosidic linkages, Quadrant 1 is the upper right (+, +), for **2** and **5** (diequatorial), Quadrant 1 is the lower left (−, −), and for compounds **3** and **4** (axial for the glycosidic, equatorial for the aglycon), Quadrant 1 is the lower right (+, −).

The analogue of α,α-trehalose (**1**) gives an adiabatic map (Figure 8) very similar to a previously determined disaccharide map [31]. It has a global minimum at $\varphi,\psi = 76°, 76°$, two identical minima in the second and third quadrants (by symmetry, at −68°, 72° and 72°, −68°), 8.7 kcal higher, and a fourth at $\varphi,\psi = -73°, -73°$, 14.9 kcal higher (Table 3). The main minimum is for a structure with both rings in $^4C_1$ conformations (**NN**), the second has one in each conformation (**AN** and **NA**), and the fourth has both rings in alternate chairs (**AA**), as observed in Table 3 and Figure 9. All the first quadrants of the individual relaxed maps (Figure 2) are almost identical, but the other quadrants are quite different. The adiabatic map has contributions from the four maps (Figure 9, Table 3), although the population of the other forms is very low (Table 5). This is expected since all the contours below 10 kcal are inside the **NN** domain (Figure 9), with the exception of small regions around the identical second and third minima ($\mathbf{E}_{rel} = 8.7$ kcal/mol). Only a few grid points led to shapes different from the original ones (Table 1), all of which started as normal chairs. The calculations starting with boat/skew forms also gave similar relaxed maps. However, none of them contributed to the adiabatic map. In the **AN**, **NA** and **AA**- dominated areas, there were many points for which the second-lowest energy corresponded to a boat form. Their energies relative to the lowest value at that point ranked as low as 0.75 kcal/mol in the **AA** domain, and 1.25 kcal/mol in the **AN/NA** domains. In any case, 99.38% of the population is from the **NN** map (Table 5).

The analogue of β,β-trehalose (**2**) shows a different behaviour [31]. In the main quadrant, the shape is quite similar to that of **1**, although inverted (Figure 8). However, the other three quadrants show much lower relative energies than in the map for **1**. In fact, only a small area of the map is above 15 kcal/mol, whereas for **1** about 40% is above 15 kcal/mol. The alternate chairs (with axial bonds) often do not keep their shapes, especially when φ or ψ are between 0 and 60°, or even in a larger region if both rings start as alternate chairs (Figure 3). This is the only compound of the six that showed this behaviour. Furthermore, the second-lowest energies at each point were at least 2.4 kcal/mol higher than the **NN** values. They were mostly **AN/NA** conformers, but some were **BN/NB** conformers that had energies 3.5 kcal or more above the lowest energy **NN** point. Again, all the relaxed maps for **2** showed very similar first quadrants, but the other quadrants were quite different. Because this adiabatic map is based entirely on **NN** conformers, one might have expected that the population of **NN** forms should have been higher than in the case of **1**, but the result is slightly reversed (Table 5). This occurs because the points that define the population are mainly those of very low energy. The **AN/NA** first quadrant minimum in **2** has a relative energy lower than 3 kcal, whereas the equivalent one in **1** is higher. This cannot be depicted by Figures 2 and 3, which show energies relative to the main minimum in each map, but Table 3 clears up this fact by showing the energy relative to the global minimum of the compound.

The adiabatic map of the analogue of α,β-trehalose (**3**) incorporated the expected behaviour, considering the results for the individual bonds in **1** and **2**. The **A** chair contributed to the adiabatic map when present in the α-linked unit, as occurred in **1**. Thus, the adiabatic map was made mainly from the **NN** relaxed map, but also (for φ values around −40°) from the **AN** relaxed map. No influence was observed from β-linked units starting in the alternate chair shape (**AA** and **NA**); those maps yielded many points with other geometries or high energies (Figure 4, Table 1). The minima in the third and fourth quadrants came from **AN** conformers (Table 3, Figure 9). Anyway, most of the **AN** domain covered high-energy regions (> 5.6 kcal, Table 3, Figure 9). Because the **AN**, **NA**, and **AA** conformers of **3** have higher relative energies than for the other five compounds, **3** exhibits the largest population of **NN** conformers (99.77%, Table 5).

The conformational energy surface of maltose has been extensively studied [28,29,32], especially in the low energy region around φ, ψ ca. 80°, −160°. Some cyclodextrins include a glucose residue with an **A** or **B** conformation [19,34–38]. The present relaxed maps show, for the first and second quadrants, a marked dependence on the conformation of the reducing unit, whereas the third and fourth quadrants showed the influence of the conformation of the non-reducing unit. In other words, for positive values of φ the conformation of the second unit defines the shape of the relaxed maps, whereas for negative values of φ, that of the first unit defines the shape. The relaxed **NN** and **AN** maps show deep minima that are close, within an expanded low-energy region of 4–5 kcal/mol. Their minima in the second quadrant have relative energies below 4 kcal/mol (Figure 5). On the other hand, the **NA** and **AA** maps show two low

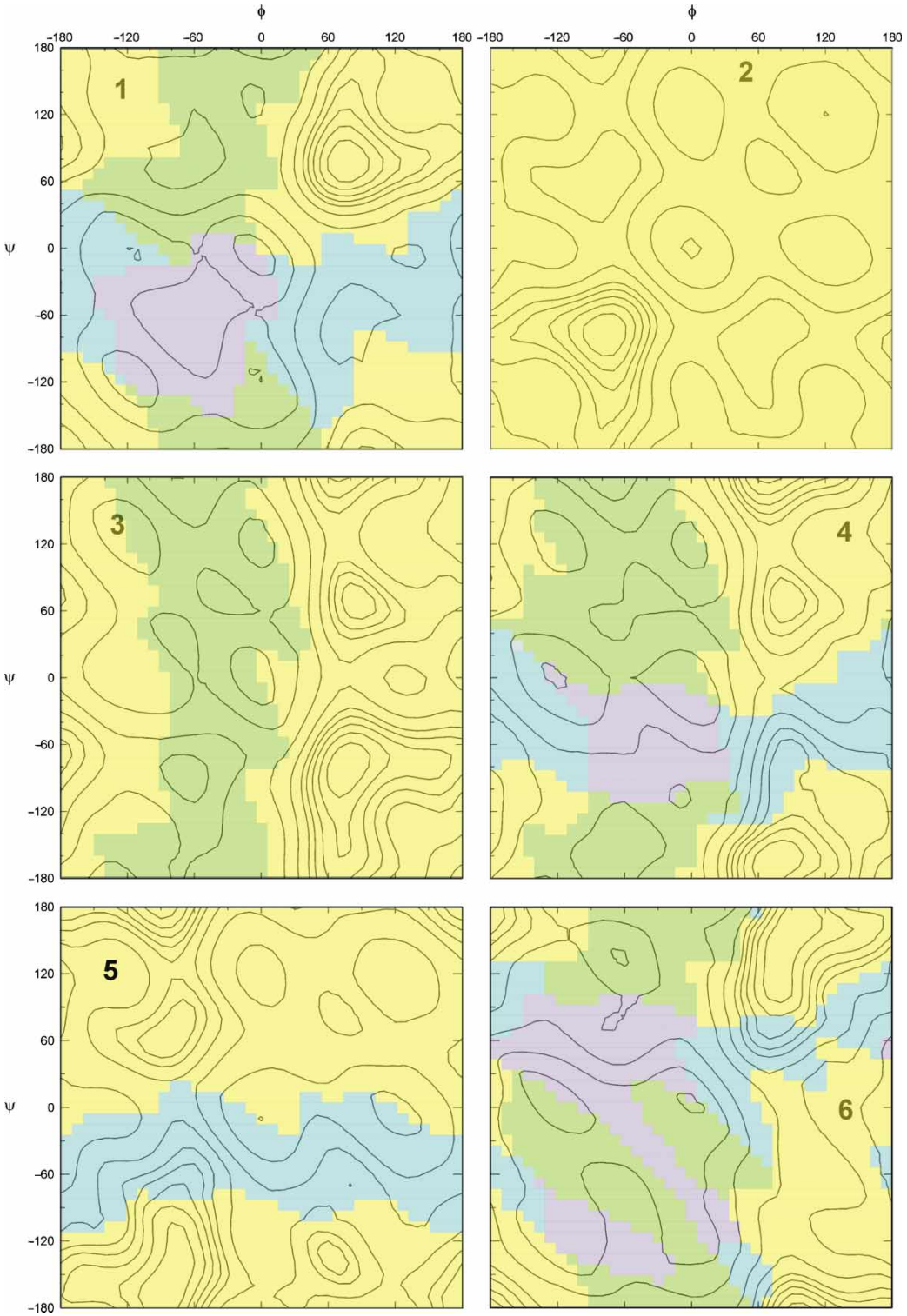

Figure 9. Colour-coded indication of the origin of points within the adiabatic contour maps of **1**–**6**. Iso-energy contour lines have 1, 2, 3, 4, 5, 7, 10, 15, 20 and 25 kcal/mol. Yellow = **NN**; Light blue = **NA**, Green = **AN**; Violet = **AA**.

Table 3. Minima determined with MM3 for compounds **1**, **2** and **3** (analogues of α,α-, β,β- and α,β-trehalose, respectively) in each quadrant, for each conformer (energies are relative to the global minimum, in kcal/mol).

	Quadrant 1	Quadrant 2	Quadrant 3	Quadrant 4
1				
AA	6.77 (77, 77) 13.38 (151,150)	12.23 (89, − 51)	12.23 (−51, 89)	14.89 (−73, − 73)
AB	7.84 (78, 75)	13.95 (83, − 60)	13.01 (−76, 64)	17.53 (−72, − 74)
AN	3.43 (78,75)	13.42 (88, − 77)	8.66 (−68, 72)	20.63 (−47, − 48)
BB	8.89 (76, 76) 14.83 (153, 153)	14.55 (76, − 62)	14.55 (−62, 76)	20.08 (−73, − 73)
BN	4.45 (76, 76) 7.93 (156, 82)	14.22 (81, − 90)	10.07 (−60, 79)	23.96 (−49, 52)
NN	0.00 (76, 76)	9.53 (85, − 72)	9.53 (−72, 85)	28.84 (−81, − 81)
2				
AA	6.91 (−76, − 76) 12.64 (−147, − 146)	19.12 (−92, 72)	19.12 (72, − 92)	–
AB	7.38 (−78, − 75) 13.24 (−119, − 160)	14.09 (−81, 62)	20.91 (72, − 91)	–
AN	2.94 (−76, − 77) 7.28 (−93, − 170)	8.13 (−84, 54)	16.55 (77, − 100)	–
BB	8.96 (−76, − 76)	15.32 (−69, 70)	15.32 (70, − 69)	22.28 (56, 56)
BN	4.52 (−76, − 76)	9.43 (−64, 75)	11.01 (68, − 74)	14.78 (65, 66)
NN	0.00 (−77, − 77) 6.57 (−151, − 150)	5.29 (−88, 52)	5.29 (52, − 88)	7.55 (73, 73)
3				
AA	6.88 (73, − 84) 8.87 (77, − 145)	–	8.88 (−69, − 90)	–
AN	4.15 (80, − 77)	5.48 (88, 67)	5.63 (−68, − 88)	13.61 (−75, 34) 13.68 (−35, 75)
NA	4.62 (71, − 127) 4.79 (146, − 76)	–	10.69 (−92, − 82)	–
NN	0.00 (75, − 80)	2.12 (86, 68)	7.42 (−89, − 81)	15.47 (−104, 59)

energy regions, one around 80°, −160° as the **NN/AN**, but another at around $\varphi,\psi = 90°, -80°$ (Table 4). The relative energy of the minimum in the second quadrant is about 5–6 kcal. In the third quadrant, only **AA/AN** maps give minima with relatively low energy (4 kcal). There are very few points that have very high energy or that result in boat conformations (Table 1). The adiabatic map is composed of **AN**, **NA**, **AA** and **NN** conformers in proportions and

Table 4. Minima determined with MM3 for compounds **4**, **5** and **6** (analogues of maltose, cellobiose and galabiose respectively) in each quadrant, for each conformer (energies are relative to the global minimum, in kcal/mol).

	Quadrant 1	Quadrant 2	Quadrant 3	Quadrant 4
4				
	6.15 (77, − 155)		10.08 (−61, − 112)	
AA	7.46 (88, − 78)	11.55 (93, 63)	10.61 (−79, − 170)	20.81 (−55, 74)
			7.43 (−77, − 173)	13.69 (−37, 80)
AN	3.34 (77, − 158)	6.59 (88, 70)	7.67 (−55, − 142)	13.85 (−74, 49)
	2.49 (76, − 154)			
NA	3.13 (86, − 76)	7.76 (88, 69)	12.26 (−78, − 116)	26.74 (−83, 51)
	0.00 (73, − 165)			18.77 (−55, 74)
NN	4.05 (157, − 115)	3.08 (85, 71)	9.70 (−62, − 142)	19.06 (−93, 66)
5				
	5.38 (−80, − 83)			
AA	7.33 (−114, − 166)	10.86 (−86, 33)	–	–
	3.15 (−94, − 173)			
AN	4.49 (−84, − 104)	7.50 (−112,57)	16.09 (95, − 157)	–
	2.42 (−77, − 85)			
NA	3.11 (−89, − 166)	7.43 (−87,37)	6.03 (61, − 127)	15.00 (65, 76)
			3.32 (64, − 135)	
NN	0.00 (−88, − 169)	3.15 (−83,61)	6.65 (27, − 172)	8.58 (70, 84)
6				
			9.63 (−61, 126)	
	5.63 (77, 81)		9.83 (−72, 75)	
AA	6.04 (88, 169)	12.68 (113, − 74)	12.76 (−28, 172)	–
		10.20 (78, − 78)		
AN	3.54 (88, 166)	10.25 (120, − 57)	6.72 (−64, 135)	16.57 (−62, − 84)
	2.11 (75, 82)			
NA	2.28 (86, 170)	7.98 (100, − 65)	11.60 (−81, 134)	–
NN	0.00 (95, 167) 0.20 (76, 114)	7.30 (116, − 56)	8.95 (−81, 144)	–

Table 5. Probability (%) of each conformation for compounds **1**–**6**.

Compound	Conf.	**AA**	**AN**	**NA**	**NN**
1	(***a,a***)	0.00	0.31	0.31	99.38
2	(***e,e***)	0.00	0.58	0.58	98.84
3	(***a,e***)	0.00	0.14	0.10	99.77
4	(***a,e***)	0.00	0.40	2.19	97.40
5	(***e,e***)	0.01	0.30	1.62	98.07
6	(***a,a***)	0.01	0.27	2.69	97.03

positions similar to those observed for **1** (Figure 9). However, here **AN** and **NA** conformers are not equivalent, and thus the former covers larger parts of the map. Paradoxically, the **NA** conformers contribute more to the total population (Table 5). This happens because its domain extends to low-energy regions, such as that of the second minimum in the first quadrant, a region that is barely above 3 kcal/mol, whereas the **AN** domain covers the minima in the third and fourth quadrants (Table 4, Figure 9).

Cellobiose has also been extensively studied [15,22,28,30,32]. The glycosidically linked unit cannot minimise in an **A** conformation throughout the entire map. Thus, some conformations in which the first unit started as **A**, finished as **N** or **B**; the other unit had no such problem (Table 1, Figure 6). Cellobiose also exhibits a two-minima behaviour in the first quadrant with some force-fields or variants [28,32]. The present study showed only one (around φ, $\psi = -90°$, $-170°$) for the **NN** relaxed map (and thus for the adiabatic one), within a very flat low-energy surface. The other three maps showed, besides the previously mentioned minimum, another one around $-80°$, $-90°$ which, for **NA** and **AA** become the global minima of the maps. This analogue shows quite different maps for each of the four conformers. The adiabatic map contains about one third of **NA** conformers. Even if none of them corresponds to a minimum on that map, their population is important (1.6%) given that it covers some low energy (4–5 kcal/mol) regions (Figure 9).

As usually occurs with α-linked disaccharides and analogues, the relaxed maps of **6** can be constructed from almost every conformation (Figure 7, Table 1). Conformers **AN** and **NN** lead to a large 0–1 kcal region with a global minimum around 90°, 170°. In one case another minimum appears at 76°, 114°, but in the other this minimum falls to the other one after strict minimisation. On the other hand, conformers with 4-linked **A** rings lead to two better-separated 1 kcal regions, for which that around 80°, 80° is the global minimum (Figure 7, Table 4). The remaining quadrants show different shapes for the four conformers. Large contributions from alternate chairs are observed in the adiabatic map (Figure 9, Table 2). However, most of them were in the high energy regions, with the exception of some **NA** conformers with energies just above 2 kcal in the main quadrant (Figure 9), probably including the minimum at 75°, 82° (the region of this minimum is just at the edge between the **NA** and **NN** domains). The **AN** conformers gave rise to the minima in the third and fourth quadrants (Table 4).

Figure 9 shows that the regions where conformers might give rise to points in the adiabatic map are independent of the configuration of the linkages. In other words, when conformers different from **NN** appear in the map, each of them usually appears at the same places (Figure 9). What can be predicted in terms of configuration is if they will appear or not: for α-linked disaccharides, a strip involving φ values from around -90 to 0° appears with contributions of the first unit as the **A** conformer. A similar contribution appears for the reducing ends with similar ψ values for either the analogues of reducing sugars (any configuration) or α-linked non-reducing disaccharides. In the area where both regions cross, **AA** conformers have the lowest energies, as expected. For the analogue of the diaxially linked disaccharide (**6**), there is more shape diversity (Figure 9).

The flexibilities observed for each of the adiabatic maps follow the trend of previous studies. However, QM calculations [18] reached much higher values, especially for the maltose analogue. It should be remembered that the present maps are for methyl-substituted tetrahydropyrans, whereas the QM maps were made with unsubstituted tetrahydropyrans that would be expected to have less steric hindrance and increased flexibilities, especially for the 1,4-linkages. Other previous work with MM3 showed very similar values for the trehalose analogues, but larger for maltose and cellobiose (Table 6). This work shows that in order to obtain a strictly adiabatic map, $^1C_4$ conformations have to be taken into account, at least for THP analogues, and working with MM3. The exact behaviour will depend on the method used to establish the potential function

Table 6. Flexibility (deg^2) for the six compounds under study, and literature data of similar compounds.

Compound	Conf.	Q	QM analogues	MM3 Disac.	MM3 Disac.	MM3 analogues	MM3 Disac.	MM3 Met. Disac.
Reference			[18]	[28]	[29–31]	[32]	[32]	[32]
1	(***a,a***)	693	811			701	635	470
2	(***e,e***)	730	1087			749	1773	715
3	(***a,e***)	924	1142					
4	(***a,e***)	836	2425	1161	1600	1451	688	820
5	(***e,e***)	1447	2025	1255	1600	1960	665	1605
6	(***a,a***)	1607	1802					

(QM, MM, which force-field or basis set, etc.), and can be a useful tool for comparing different potential expressions. The possibility of unexpected flipping of the normal ring forms has already been suggested in other analogues [33,36]. It is certainly possible that real disaccharides, with their numerous hydroxyl groups, will behave differently from these analogues. In the case of glucose itself, the large number of equatorial hydroxyl groups may hinder the achievement of low-energy alternate ring forms. However, with other sugars, this possibility can become more important. On the other hand, hydrogen-bonding may stabilise either normal or alternate chairs in regions of the map where these analogues do not appear to be stabilised. In any case, ring shape appears to be another manifestation of the "multiple minima problem" [2,5].

5. Computational methods

Molecular mechanics calculations were carried out at the University of Buenos Aires using the program MM3(92) (QCPE, Indiana University, USA) [23], with relevant parameters modified as in the MM3(2000) version [39]. Also, the maximum atomic movement at each step of the minimisation was reduced from 0.25 to 0.10 Å. The dielectric constant was 1.5 (the MM3 default for an isolated molecule). This level of theory was deemed adequate for the demonstration purposes of the present work. Structures at grid points were minimisations using the block diagonal method, with a termination condition one hundred times tighter than the MM3 default. For the minima, full-matrix minimisations were made to check that they correspond to true minima, after several successive block diagonal calculations starting from neighbouring grid points. This verified that a nearly flat surface that ultimately leads to another minimum is not present. The starting structures for the sugar analogues were generated by sketching and minimising conformers in the appropriate chair (or boat) conformation, and then the glycosidic angle was set to 150° [6]. From each of those starting structures, relaxed maps were obtained by changing both φ and ψ in 10° steps, leading to 1296 final structures. The grid was scanned with the MM3 dihedral driver 4 (each grid point is generated from the original starting structure rather than using an optimised structure from a previous grid point). The adiabatic maps were constructed by using, for each grid point, the lowest energy value for each set of relaxed maps. The contribution of each relaxed map (or starting geometry) to the adiabatic map was evaluated from their probability distributions assuming no entropic differences:

$$P_i = \frac{\sum_{\phi_\varphi}^{1296} e^{-E\phi_\varphi i/RT}}{\sum_{i=1}^{4}\sum_{\phi_\varphi}^{1296} e^{-E\phi_\varphi i/RT}}$$

i.e. the ratio of the Boltzmann populations summed over each entire relaxed map normalised for the four maps ($i = 1$–9 for **1** and **2**, see below). The molecular flexibility [18,27,33] was calculated from the partition function for the adiabatic map:

$$q = \Delta\phi \times \Delta\psi \times \sum_{i=1}^{1296} e^{-(Ei-Egm)/RT}$$

where $\Delta\phi$ and $\Delta\psi$ are the grid spacings (10° each in this case) and the summation is carried out over the entire ϕ, ψ surface (1296 points).

Acknowledgements

This work was supported by grants from CONICET (PIP 5699), UBA (X-174), and normal research funds of the US Department of Agriculture. CAS is a Research member of the National Research Council of Argentina (CONICET).

Note

1. In this context, "relaxed" means that the atoms were free to move to a position that corresponded to the nearest local minimum in the potential energy surface, except for the linkage torsión angles which were restrained to a particular φ, ψ combination. This "relaxation" does not imply at all a comprehensive search for the orientations of the exocyclic groups or the ring shapes.

References

[1] S. Pérez, *Theoretical aspects of oligosaccharide conformation*, Curr. Opin. Struct. Biol. 3 (1993), p. 675.
[2] A.D. French and J.W. Brady, *Computer modeling of carbohydrates*, ACS Symp. Ser. 430 (1990), p. 1.
[3] V. Tran, A. Bulèon, A. Imberty, and S. Pérez, *Relaxed potential energy surfaces of maltose*, Biopolymers 28 (1989), p. 679.
[4] A.D. French and M.K. Dowd, *Exploration of disaccharide conformations by molecular mechanics*, J. Mol. Struct. (Theochem.) 286 (1993), p. 183.
[5] C.A. Stortz, *Disaccharide conformational maps: how adiabatic is an adiabatic map?* Carbohydr. Res. 322 (1999), p. 77.
[6] A.D. French, A.-M. Kelterer, G.P. Johnson, M.K. Dowd, and C.J. Cramer, *Constructing and evaluating energy surfaces of crystalline disaccharides*, J. Mol. Graph. Model. 18 (2000), p. 95.
[7] S. Melberg and K. Rasmussen, *Conformations of disaccharides by empirical force-field calculations. Part I, β-maltose*, Carbohydr. Res. 69 (1979), p. 27.
[8] ———, *Conformations of disaccharides by empirical force-field calculations. Part II, β-cellobiose*, Carbohydr. Res. 71 (1979), p. 25.
[9] ———, *Conformations of disaccharides by empirical force-field calculations. Part III, β-gentiobiose*, Carbohydr. Res. 78 (1980), p. 215.
[10] I. Tvaroška and S. Pérez, *Conformational energy calculations for oligosaccharides: a comparison of methods and a strategy of calculation*, Carbohydr. Res. 149 (1986), p. 389.
[11] A.D. French, *Rigid- and relaxed-residue conformational analyses of cellobiose using the computer program MM2*, Biopolymers 27 (1988), p. 1519.

[12] S.N. Ha, L.J. Madsen, and J.W. Brady, *Conformational analysis and molecular dynamics simulations of maltose*, Biopolymers 27 (1988), p. 1927.

[13] A.D. French, *Comparison of rigid and relaxed conformational maps for cellobiose and maltose*, Carbohydr. Res. 188 (1989), p. 206.

[14] A. Imberty, V. Tran, and S. Pérez, *Relaxed potential energy surfaces of* n*-linked oligosaccharides: the mannose-α-(1 → 3)-mannose case*, J. Comput. Chem. 11 (1989), p. 205.

[15] A.D. French and G.P. Johnson, *Roles of starting geometries in quantum mechanics studies of cellobiose*, Mol. Simul., 34, (2008), p. 365.

[16] I. Tvaroška and L. Václavík, *Stereochemistry of nonreducing disaccharides in solution*, Carbohydr. Res. 160 (1987), p. 137.

[17] P. Zhang, A.N. Klymachyov, S. Brown, J.G. Ellington, and P.J. Grandinetti, *Solid-state* ^{13}C *NMR investigations of the glycosidic linkage of α-α′trehalose*, Solid State Nucl. Magn. Reson. 12 (1998), p. 221.

[18] A.D. French, A.-M. Kelterer, G.P. Johnson, M.K. Dowd, and C.J. Cramer, *HF/6-31G* Energy surfaces for disaccharide analogs*, J. Comput. Chem. 22 (2001), p. 65.

[19] T. Steiner and W. Saenger, *Closure of the cavity in permethylated cyclodextrins through glucose inversion, flipping, and kinking*, Angew. Chem. Int. Ed. 37 (1998), p. 340.

[20] A.D. French, G.P. Johnson, A.-M. Kelterer, M.K. Dowd, and C.J. Cramer, *Quantum mechanics studies of the intrinsic conformation of trehalose*, J. Phys. Chem. A 106 (2002), p. 4988.

[21] C.O. da Silva and M.A. C. Nascimento, Ab initio *conformational maps for disaccharides in gas phase and aqueous solution*, Carbohydr. Res. 339 (2004), p. 113.

[22] A.D. French and G.P. Johnson, *Quantum mechanics studies of cellobiose conformations*, Can. J. Chem. 84 (2006), p. 603.

[23] N.L. Allinger, Y.H. Yuh, and J.-H. Lii, *Molecular mechanics. The MM3 force field for hydrocarbons*, J. Am. Chem. Soc. 111 (1989), p. 8551.

[24] M.K. Dowd, A.D. French, and P.J. Reilly, *Modeling of aldopyranosyl ring puckering with MM3(92)*, Carbohydr. Res. 264 (1994), p. 1.

[25] X. Biarnés, A. Ardèvol, A. Planas, C. Rovira, A. Laio, and M. Parrinello, *The conformational free energy landscape of β-*D*-glucopyranose. Implications for substrate preactivation in β-glucoside hydrolases*, J. Am. Chem. Soc. 129, (2007), p. 10686.

[26] D. Cremer and J.A. Pople, *A general definition of ring puckering coordinates*, J. Am. Chem. Soc. 97 (1975), p. 1354.

[27] C.A. Stortz, *Potential energy surfaces of carrageenan models: carrabiose, β-(1 → 4)-linked* D*-galactobiose, and their sulfated derivatives*, Carbohydr. Res. 337 (2002), p. 2311.

[28] C.A. Stortz and A.S. Cerezo, *Depicting the MM3 potential energy surfaces of trisaccharides by single contour maps: application to β-cellotriose and α-maltotriose*, Carbohydr. Res. 338 (2003), p. 95.

[29] M.K. Dowd, J. Zeng, A.D. French, and P.J. Reilly, *Conformational analysis of the anomeric forms of kojibiose, nigerose, and maltose using MM3*, Carbohydr. Res. 230 (1992), p. 223.

[30] M.K. Dowd, A.D. French, and P.J. Reilly, *Conformational analysis of the anomeric forms of sophorose, laminaribiose, and cellobiose using MM3*, Carbohydr. Res. 233 (1992), p. 15.

[31] ———, *Conformational analysis of trehalose disaccharides and analogues using MM3*, J. Comput. Chem. 13 (1992), p. 102.

[32] S. Mendonca, G.P. Johnson, A.D. French, and R.A. Laine, *Conformational analyses of native and permethylated disaccharides*, J. Phys. Chem. A 106 (2002), p. 4115.

[33] C.A. Stortz and A.S. Cerezo, *Potential energy surfaces of α-(1 → 3)-linked disaccharides calculated with the MM3 force-field*, J. Carbohydr. Chem. 21 (2002), p. 355.

[34] M. Añibarro, K. Gessler, I. Uson, G.M. Sheldrick, K. Harata, K. Uekama, F. Hirayama, Y. Abe, and W. Saenger, *Effect of peracylation of β-cyclodextrin on the molecular structure and on the formation of inclusion complexes: an X-ray study*, J. Am. Chem. Soc. 123 (2001), p. 11854.

[35] K. Harata, F. Hirayama, H. Arima, K. Uekama, and T. Miyaji, *Crystal structure of heptakis (2,3,6-tri-*O*-methyl)-β-cyclodextrin complexes with* m*-iodophenol and 4-biphenylacetic acid. Guest-induced conformational change of a pyranose ring*, J. Chem. Soc. Perkin Trans. 2, (1992), p. 1159.

[36] A.D. French, G.P. Johnson, A.-M. Kelterer, and G.I. Csonka, *Fluorinated cellobiose and maltose as stand-ins for energy surface calculations*, Tetrahedron: Asymmetry 16 (2005), p. 577.

[37] G.P. Johnson, E.D. Stevens, and A.D. French, *Octa-*O*-propanoyl-β-maltose: crystal structure, acyl stacking, related structures, and conformational analysis*, Carbohydr. Res. 342 (2007), p. 1210.

[38] A.D. French and G.P. Johnson, *Linkage and pyranosyl ring twisting in cyclodextrins*, Carbohydr. Res. 342 (2007), p. 1223.

[39] C.A. Stortz, *Comparative performance of MM3(92) and two Tinker MM3 versions for the modeling of carbohydrates*, J. Comput. Chem. 26 (2005), p. 471.